Olorofim and the azoles are antagonistic in *A. fumigatus* and functional genomic screens reveal mechanisms of cross resistance.

Authors: Norman van Rhijn[1,2], Sam Hemmings[1], Clara Valero[1,3], Jorge Amich[1], Michael J Bromley[1,2]

[1] Manchester Fungal Infection Group, Division of Evolution, Infection, and Genomics, Faculty of Biology, Medicine and Health, University of Manchester, CTF Building, 46 Grafton Street, Manchester, M13 9NT, UK.

[2] Antimicrobial Resistance Network, University of Manchester, Manchester M13 9PT, UK

[3] Faculdade de Ciências Farmacêuticas de Ribeirão Preto, Departamento de Ciências Farmacêuticas, Universidade de São Paulo, Avenida do Café S/N, Ribeirão Preto 14040-903, Brazil.

*To whom correspondence should be addressed:

Michael J Bromley, Phone: (+44) (0)161 275 1703, email: mike.bromley@manchester.ac.uk

Keywords: Aspergillus fumigatus, Olorofim, Orotomide, Antimicrobial resistance, Antifungal, Transcription factor, Aspergillosis, Nitrogen metabolism, Antagonism

Abstract:

Aspergillosis, in its various manifestations, is a major cause of morbidity and mortality. Very few classes of antifungal have been approved for clinical use to treat these diseases and resistance to the first line therapeutics is increasing. A new class of antifungals, the orotomides, are currently in development with the first compound in this class olorofim in late-stage clinical trials. In this study, we characterise a network of genes that govern olorofim response in *A. fumigatus*. We reveal that the number of transcription factors that regulate olorofim susceptibility are far fewer than we have previously observed for the azoles and the change in sensitivity observed in these isolates is less extreme. Intriguingly, loss of function in two higher order transcriptional regulators, HapB a member of the heterotrimeric HapB/C/E (CBC) complex or the regulator of nitrogen metabolic genes AreA, leads to cross resistance to both the azoles and olorofim. However, a clinical azole resistant isolate with a point mutation in HapE ($hapE^{P88L}$) retains sensitivity to olorofim. Our transcriptomic analysis suggests that altered sensitivity to olorofim may emerge via modification of genes involved in the production of pyrimidine biosynthetic precursors. Finally, we also show that the action of the azoles are antagonistic to olorofim *in vitro*.

33 **Introduction:**

34 Invasive and chronic forms of aspergillosis affect over 3 million people resulting in excess of
35 300 thousand deaths per year [1]. Only three classes of antifungals are currently clinically
36 available to treat aspergillosis, with the triazoles used as first-line therapy in most centres [2].
37 Resistance to the azoles is rising, which is linked to usage of triazole compounds in agri- and
38 horticulture [3]. It is expected more resistant *A. fumigatus* will be seen due to increased azole
39 used in farming linked to climate change [4]. In the last decade, isavuconazole is the only
40 antifungal to have been approved by the Food and Drug Administration (FDA) for treatment
41 of invasive aspergillosis [5], however many of the mechanisms that contribute to resistance to
42 the other azoles also result in isavuconazole resistance. The development of novel classes of
43 antifungals will be a key component to addressing the emerging resistance problem.
44 Fortunately, there are a number of novel classes of antifungal currently in development for
45 treatment of invasive aspergillosis (IA) including ibrexafungerp, which has recently (2021)
46 gained FDA approval for treatment of vulvovaginal candidiasis and olorofim (phase 3) [6].
47 Olorofim (formerly known as F901318 and under development by F2G, Ltd.) is of particular
48 interest as it is not only a member of a novel class of antifungal (the orotomides) but unlike
49 ibrexafungerp has a novel mechanism of action that has not been exploited clinically [7]. As
50 olorofim is orally bioavailable it presents a realistic alternative to the azoles for long-term
51 treatment of chronic and allergic infections and especially resistant infections [8] and could
52 potentially be used in combination therapy strategies to supress the emergence of resistance.

53

54 Olorofim acts by inhibiting the enzyme dihydroorotate dehydrogenase (DHODH), which is a
55 crucial enzyme within the pyrimidine biosynthesis pathway and is required for both DNA and
56 RNA synthesis [7]. Structural and biochemical analysis of DHODH suggests olorofim
57 competes with CoQ to bind to DHODH, preventing the oxidation of dihydroorotate to orotate.

58 DHODHs are grouped into 2 classes according to sequence similarity and subcellular
59 localisation. Both mammals and most fungi have class 2 DHODH, which is bound to the inner
60 mitochondrial membrane [9]. The human DHODH only shares 30% protein sequence identity
61 with the *A. fumigatus* DHODH and olorofim has also been demonstrated to be >2,200-fold
62 more potent against the *A. fumigatus* enzyme [7]. Inhibition of the pyrimidine biosynthesis
63 pathway by olorofim prevents the germination of *A. fumigatus* conidia and causes hyphae to
64 undergo morphological changes [10]. Prolonged exposure of germlings and vegetative hyphae
65 to olorofim also causes extensive isotropic expansion that is then followed by cell lysis [11].
66
67 Olorofim has an effect on a wide range of fungi and has been shown to be effective against
68 *Coccidioides immitis*, *Scedosporium* spp., *Madurella mycetomatis*, *Lomentospora prolificans*
69 and several *Aspergillus* species [12-18]. Olorofim is also effective against triazole resistant *A.*
70 *fumigatus* isolates and cryptic *Aspergillus* species [19, 20]. In several murine models of
71 aspergillosis, olorofim treatment significantly reduced fungal burden and mortality [15].
72 However, olorofim has a reduced activity against *Fusarium solani* species complex and
73 *Fusarium dimerum* and is inactive against Mucorales [21]. To date, there is no reported
74 incidence of acquired olorofim resistance in clinical isolates of normally susceptible fungal
75 species.
76 In this study, we explore potential routes to olorofim resistance for *A. fumigatus* through
77 screening a 484-member *A. fumigatus* transcription factor null mutant library. We have
78 uncovered a total of four transcription factors, which regulate susceptibility to olorofim.
79 Existing published literature, and our phenotypic and transcriptomic data revealed these
80 transcription factors regulate genes involved in upstream processes of the pyrimidine
81 biosynthesis pathway. Notably two of these transcription factor null mutants, Δ*hapB* and
82 Δ*areA,* had elevated MICs to olorofim and are resistant to the azole class of antifungal

83 highlighting potential routes to cross resistance. As HapB is a member of the heterotrimeric
84 CCAAT-binding complex (which comprises HapB/C and E) we assessed the susceptibility of
85 a azole resistant clinical isolate with a mutation in *hapE* (*HapE*^{P88L}). Intriguingly this mutation
86 does not change susceptibility towards olorofim. Furthermore, we demonstrate that there is an
87 antagonism between the azoles and olorofim in three wild-type strains of *A. fumigatus* and the
88 olorofim resistant mutants. Despite our discovery that there are mechanisms that can reduce
89 susceptibility to both azoles and orotomides we feel these results do not preclude the
90 development of combination therapeutics with these two agents. Our study also provides data
91 that can be used to develop molecular diagnostic tests to identify olorofim resistant isolates in
92 clinic.
93

94 **Materials and Methods:**

95 *Fungal strains*

96 Conidia of *Aspergillus fumigatus* MFIG001 (a derivative of CEA10) and transcription factor
97 null mutants [22, 23] were prepared by inoculating strains in vented 25cm^2 tissue culture flasks
98 with Sabouraud Dextrose agar (Oxoid, Hampshire, England) and incubating at 37°C for 48
99 hours. Spores were harvested in PBS + 0.01% Tween-20 by filtration through Miracloth.
100 Spores were counted using a haemocytometer (Marienfeld Superior, Baden-Württemberg,
101 Germany). The clinical isolate VP067-36, containing the P88L allele of HapE, was a kind gift
102 from Willem Melchers and Paul Verweij [24]. To construct the HapE^{P88L} allele in MFIG001,
103 the *hapE* gene was amplified from VP067-36 using primers hapE_gene_Fw and
104 hapE_gene_Rv (**Supplementary Table 1**). This PCR product was transformed into *A.*
105 *fumigatus* MFIG001 using CRISPR-Cas9 mediated transformation, using hapE_392_revcom
106 as crRNA [25]. Transformants were selected using voriconazole (1 mg/L) containing YPS
107 plates. Transformation was confirmed by PCR amplification of the complete *hapE* gene
108 (hapE_Fw and hapE_Rv), followed by Sanger sequencing using hapE_Seq.

109 *Olorofim MIC screening*

110 Olorofim was a kind gift of F2G Ltd. The Minimum Inhibitory Concentration (MIC) of
111 olorofim against *A. fumigatus* was assessed using the European Committee for Antimicrobial
112 Susceptibility Testing (EUCAST) methodology [21, 26]. Briefly, 2x10^4 spores/mL (in 100 µl)
113 were added to a CytoOne® 96-well plate (StarLab, Brussels, Belgium) containing 1xRPMI-
114 1640 medium (Sigma Aldrich, St. Louis, MO), 165 mM MOPS buffer (pH 7.0), 2% glucose,
115 with olorofim 2-fold dilution series ranging from 0.1 µg/L to 0.25 mg/L and a drug free control
116 (n = 4). Additionally, a serial dilution of olorofim containing 10 mM uracil and uridine was
117 performed. 96-well plates were incubated at 37°C for 48 hours. The MIC was determined as
118 the minimum drug concentration at which no germination was observed. Optical density was

119 measured at 600 nm using a Synergy™ HTX Multi-Mode Microplate Reader (BioTek,
120 Winooski, VT). In keeping with research laboratory based definitions, but in contract to
121 definitions used clinically, we define *in vitro* resistance as a strain that is less susceptible to
122 drug than the parental isolate [27].

123 *Olorofim sensitivity screening of the A. fumigatus transcription factor null mutant library*

124 $2x10^4$ spores/mL from each of the 484 members of the transcription knockout library were
125 added to 1x RPMI-1640 medium, 165 mM MOPS buffer (pH 7.0), 2% glucose in each well of
126 a CytoOne® 96-well plate with 0.002 mg/L olorofim (n = 4). Plates were incubated at 37°C for
127 48 hours. Fitness was calculated by dividing the optical density of respective null mutants to
128 the MFIG001 control. Relative fitness in olorofim was calculated by dividing fitness in
129 olorofim with general growth fitness of the transcription factor null mutants using the same
130 microculture conditions in 1x RPMI-1640 medium, 165 mM MOPS buffer (pH 7.0), 2%
131 glucose without olorofim (n = 4). Optical density was measured at 600 nm on a Synergy™
132 HTX Multi-Mode Microplate Reader (BioTek, Winooski, VT).

133 *RNA-extraction*

134 $1x10^6$ spores/mL of *A. fumigatus* MFIG001, Δ*AFUB_056620* and Δ*AFUB_030440* were
135 inoculated into 50 mL of *Aspergillus* complete media (ACM) [28] and incubated for 18 hours
136 at 37°C in a rotary shaker (180 rpm). Mycelia were harvested using filtration through Miracloth
137 (Merck Millipore) and washed in 1x RPMI-1640 medium. Approximately 1g of mycelia was
138 added to shake flasks containing 50 mL RPMI-1640 medium, 165 mM MOPS buffer (pH 7.0),
139 2% glucose and incubated for 1 hour at 37°C in a rotary shaker (180rpm) in the presence or
140 absence of 0.062 mg/L olorofim (n = 3). Mycelia was filtered through Miracloth and
141 snapfrozen using liquid nitrogen and kept at -80°C until required.

142 To extract RNA, 1 mL of TRIzol reagent (Sigma Aldrich) and 710-1180 µm acid washed glass
143 beads (Sigma Aldrich) were added to frozen mycelia and placed in a TissueLyser II® (Qiagen,

144 Hilden, Germany) for 3 minutes at 30 Hz. The solution was centrifuged (12,000 rpm) for 1
145 minute at 4°C. The aqueous phase was added to 200 µL of chloroform and centrifuged (12,000
146 rpm) for 10 minutes at room temperature. The supernatant was added to 0.2 M sodium citrate,
147 0.3 M sodium chloride and 25% (v/v) isopropanol and left at room temperatures for 10 minutes.
148 This solution was centrifuged (12,000 rpm) for 15 minutes at 4°C. The supernatant was
149 removed; the pellet was washed in 70% (v/v) ethanol and resuspended in RNase free water
150 (Thermo Fisher Scientific, Waltham, MA). RNA samples were treated with RQ1 RNase-Free
151 DNase (Promega, Madison, WI) and purified using a RNeasy Mini Kit (Qiagen). RNA quality
152 and quantity were assessed using gel electrophoresis and using a NanoDrop™ 2000/2000c
153 Spectrophotometer (Thermo Fisher Scientific). All RNA extractions were carried out in
154 triplicate.

155 *Transcriptomic Analysis*

156 RNA sequencing was carried out by the Genomic Technologies Core Facility (GTCF) at The
157 University of Manchester. Sequencing libraries were prepared from mRNA using TruSeq®
158 Stranded mRNA assay (Illumina, San Diego, CA). Samples were sequenced on a single lane
159 on an Illumina HiSeq2500 (Illumina). Low-quality reads of resulting fastq files were removed
160 using FastQC and trimmed using Trimmomatic (Quality >20, Sliding window average of 4
161 bases) [29]. Bowtie was used to align libraries to the *A. fumigatus* A1163 genome assembly
162 GCA_000150145.1 with gene annotation from CADRE/Ensembl Fungi v24 [30]. Differential
163 expression analysis of was performed using DESeq2 [31].

164 Functional category and gene ontology enrichment analysis was carried out using FungiFun2
165 2.2.8, converting genes to Af293 gene names to allow using the KEGG option [32]. Genes that
166 showed over 2-fold in differential expression and Benjamin-Hochberg FDR <0.01 underwent
167 enrichment analysis. StringsDB analysis was performed by only including genes with at least
168 two connections.

169 *Phenotypic analysis*

170 For colony images, 500 spores per isolate were spotted onto solid ACM or Aspergillus Minimal
171 Media (AMM) and left to dry. Plates were incubated at 37°C for 72 hours and imaged. Growth
172 on solid AMM supplemented with different nitrogen sources (50 mM ammonium tartrate, 10
173 mM sodium nitrate, 10 mM L-glutamine, 10 mM urea or 10 mM L-proline) were assessed by
174 spotting 500 spores from each isolate (n = 3). Plates were incubated at 37°C for 72 hours. MICs
175 were determined using the same supplementation as the phenotypic test with a serial dilution
176 of olorofim (ranging from 0.1 µg/L to 0.25 mg/L). 96-well plates were incubated for 48 hours
177 at 37°C and growth was determined by microscopic evaluation.

178 *Checkerboard assays*

179 For assessing drug combination efficacies of itraconazole and olorofim against *A. fumigatus*,
180 we used a checkerboard assay similar to EUCAST MIC testing described above. Twofold serial
181 dilutions of itraconazole were prepared across the X-axis and olorofim serial dilutions across
182 the Y-axis. The MIC was determined by microscopy by visually assessing the well containing
183 the lowest drug concentration with non-germinated spores. The fractional inhibitory
184 concentration index (FICI) was calculated as the MIC in combination divided by the MIC of
185 individual drugs [33].

186

187 *Disk assays*

188 4×10^4 conidia of the relevant *A. fumigatus* strain were evenly distributed on solidified 1xRPMI
189 1640 (Sigma), 165 mM MOPS buffer (pH 7.0), 2% glucose. One 6 mm antibiotic assay disk
190 (Whatman) was placed on the middle of the plate or two disks at a fixed distance, and 10 µL
191 of voriconazole (0.8 mg/mL), olorofim (0.005 mg/L) or H_2O_2 (30%) were added to each of
192 them. The plates were incubated at 37°C for 48 hours and imaged.

193

Data availability

RNA-seq data is available from ArrayExpress as experiment: E-MTAB-10590. The differential expression output from DESeq2 is included as Supplementary Data 1. (reviewer access: Reviewer_E-MTAB-10590 Password: pptwwqmj)

Acknowledgements

The authors would like to thank F2G for supplying the drug. We would also like to thank the Genomic Technology Core Facility, the Bioinformatics Core Facility in the University of Manchester for their technical support. This work was supported by the Wellcome Trust grant number 219551/Z/19/Z and 208396/Z/17/Z to M.B. CV is funded by postdoctoral fellowship from Fundação de Amparo à Pesquisa do Estado de São Paulo (FAPESP-BEPE 2020/01131-5).

Competing interests

Michael Bromley is a former employee of F2G Ltd. F2G currently funds a PhD position in the laboratory. F2G was not involved in any of the experimentation or analysis of data in this study.

Author contributions

N.v.R designed and performed the experiments, analysis, wrote and edited the manuscript. S.H. designed and performed experiments and analysis. C.V. designed and performed experiments and analysis. J.A. designed and performed experiments and analysis. M.B. provided the funding, designed the experiments, wrote and edited the manuscript

Results:

The effect of olorofim on A. fumigatus MFIG001 results in minor transcriptional changes in the pyrimidine biosynthetic pathway.

In order to standardise assays throughout, the Minimum Inhibitory Concentration (MIC) of olorofim against *Aspergillus fumigatus* MFIG001 was determined. The MIC was defined as the minimum concentration of olorofim at which no germination from *Aspergillus* spores was observed by microscopic evaluation (**Supplemental Figure 1**). Microscopic evaluation revealed the MIC of olorofim to be 0.06 mg/L for *A. fumigatus* MFIG001, consistent with previous findings of other *A. fumigatus* isolates [19]. The effect of olorofim on growth of *A. fumigatus* was further evaluated by measuring optical density of the plates used to determine the MIC (**Figure 1a**). The maximal growth observed (OD_{600} = 0.39) and minimal growth observed (OD_{600} = 0.04) was separated by a 64-fold difference in drug concentration, which is in stark contrast to the inhibitory effects of the azoles on *A. fumigatus* where the difference between maximal and minimal growth typically occurs over a drug concentration not exceeding 8-fold (**Supplemental Figure 2**). As this range is so broad, we consider it useful to measure the concentration at which growth is inhibited by 50% (herein referred to as IC50 [34] to distinguish from MIC50 which is an MIC determination made of populations). For MFIG001, the IC50 for olorofim is 0.012 mg/L whereas for itraconazole its 0.65 mg/L [22]. As olorofim inhibits pyrimidine biosynthesis, it would be expected that the action of the drug would be fully reversed by supplementing the media with an excess of exogenous pyrimidines [7]. To confirm growth inhibition was due to directly targeting the pyrimidine biosynthesis pathway, the MIC was determined with the addition of 10 mM uridine and 10 mM uracil

242 (**Figure 1b**). Under these conditions there was no observed reduction in *A. fumigatus* growth,
243 and at all olorofim concentrations the median OD_{600} did not fall below control levels indicating
244 that there are no significant off target effects of this drug.
245 To facilitate our understanding of how olorofim impacts the transcriptome of *A. fumigatus*,
246 RNA-seq analysis was performed. Upon olorofim exposure (1x MIC), a modest 185 genes and
247 41 genes respectivley were up- and downregulated (**Figure 1c**). Our expectation was that
248 several genes in the immediate pyrimidine biosynthesis pathway would be upregulated
249 however only the multifunctional carbamoyl-phosphate synthase/aspartate
250 carbamoyltransferase (PyrABCN, AFUB_077330) enzyme, which is upstream of DHODH and
251 converts carbamoyl-P to N-carbamoyl-L-aspartate, was upregulated by Log2 fold >1. Instead,
252 genes associated with pathways that synthesise precursors of the pyrimidine biosynthetic
253 pathway were identified including oxaloacetate metabolism and glutamate biosynthesis
254 (**Figure 1d,e**). Genes associated with tyrosine metabolism; secondary metabolite biosynthesis,
255 glycolysis/gluconeogenesis and valine, leucine and isoleucine degradation were enriched
256 among downregulated genes (**Figure 1d,e**). Interestingly, several proteins involved in
257 ergosterol biosynthesis (HmgA, Erg13a and Erg26) were differentially expressed
258 (**Supplemental Data 1**).
259 ***Deletion of HapB, AreA, DevR and AcdX changes olorofim susceptibility.***
260 In order to identify novel transcriptional regulators associated with differential olorofim
261 susceptibility, the COFUN transcription factor knockout (TFKO) library was screened against
262 olorofim at a concentration that reduces growth of the isogenic wildtype isolate (MFIG001) by
263 c 20% (0.002 mg/L). At this concentration we were able to identify strains that have the
264 potential to be resistant or hypersensitive (**Figure 2a**).
265

266 Three transcription factor null mutants (Δ*areA,* Δ*hapB* and Δ*devR*) showed reproducible
267 increased relative fitness in the presence of olorofim and elevated MICs compared to MFIG001
268 (**Figure 2c, d and e**). Remarkably, two of these mutants (Δ*areA* and Δ*hapB*) are also resistant
269 to the azole class of antifungals. Loss of AreA, a transcription factor that has a global role in
270 activating expression of genes involved in nitrogen acquisition and processing [35] or loss of
271 HapB, which along with HapC and HapE, comprise the CCAAT Binding Complex (CBC) [36]
272 resulted in a 2-fold increase in MIC to olorofim when compared to the isotype control
273 MFIG001; IC50 values for these strains were 0.04 mg/L (4-fold increase) and 0.07 mg/L (8
274 fold-increase), respectively (**Figures 2c and 2e**). The Δ*devR* mutant showed a significant
275 reduction in susceptibility to olorofim at concentrations ranging from 0.008 mg/L to 0.06 mg/L
276 (MIC) and had an IC50 of 0.025 mg/L (**Figure 2d**). Although the MIC for this strain increased
277 to >0.125 mg/L most spores did not germinate at this concentration making this phenotype
278 reminiscent of tolerance **(Supplemental Figure 1)**.
279 One isolate (ΔAFUB_056620, Δ*acdX*) showed a significant increase in sensitivity to olorofim
280 and had an MIC of 0.03 mg/L and a IC50 of 0.006 mg/L, 2-fold lower than *A. fumigatus*
281 MFIG001 (**Figure 2b**). The *acdX* gene encodes a 612 amino acid transcription factor which, a
282 SMART domain search showed, contains six WD40 repeat units but no other functional
283 domains. A reciprocal BLAST of the AFUB_056620 protein sequence found a match to the
284 *Saccharomyces cerevisiae* transcription factor Spt8. However, the proteins only share 44%
285 identity of the entire protein sequence. In *S. cerevisiae*, Spt8 forms part of the SAGA (Spt-
286 Ada-Gcn5-acetyltransferase) complex [37] which is known to act as a transcriptional activator
287 under several stress conditions. While the orthologue of AcdX in other fungi generally contains
288 six WD40 domains, in species such as *N. crassa* and *A. terreus* only five domains are present,
289 however the significance of this is unclear. In *A. nidulans* AcdX has been described to be

290 functional in the SAGA complex and is involved in repressing genes in in acetate metabolism
291 and has a regulatory role in the proline metabolic pathway [38].
292
293 ***Transcription factor mutants with altered suseptibility to olorofim have defects in nitrogen***
294 ***assimilation.***
295 Further phenotypic analysis of the null mutants with differential susceptibility to olorofim
296 revealed that all had growth defects on *Aspergillus* Complete Medium (ACM) (**Figure 3a and**
297 **b**) and *Aspergillus* Minimal Medium (AMM) (**Figure 3a and c**). The *hapB, devR, areA* and
298 *acdX* null mutants showed a reduction of radial growth on ACM of 28%, 22%, 12% and 24%
299 respectively when compared to the isotype control. On AMM, the *hapB* mutant showed
300 increase radial growth (58%) however, colony growth was more diffuse than the isotype strain
301 (**Figure 3a and c**). As olorofim inhibits DHODH, which acts within the pyrimidine
302 biosynthetic pathway, and we observed that olorofim results in transcriptional repositioning of
303 several pathways linked to nitrogen processing we hypothesised that these growth defects could
304 be nitrogen source dependent. Indeed, the radial growth defect of strains were reversed by
305 differential supplementation (Δ*devR* by proline*;* Δ*acdX* by glutamine or proline and Δ*areA* by
306 glutamine). Furthermore, we observed an interesting correlation between radial growth on the
307 different nitrogen containing media and olorofim sensitivity. While the radial growth of the
308 isotype isolate differed little between nitrogen sources (**Figure 3d and Supplemental Figure**
309 **3**) the strains lacking the ability to effectively utilise nitrate as a sole nitrogen source were all
310 less susceptible to olorofim. Taken together, this suggests that defects in nitrogen utilisation in
311 these transcription factor null mutants could be linked to their olorofim susceptibility.
312 ***Changes in susceptibility to olorofim in* Δ*devR* and Δ*acdX* mutants *are caused by opposing***
313 ***regulation of pathways preceding pyrimidine biosynthesis***

314 In order to characterise the basis of differential olorofim susceptibility in the Δ*devR* and Δ*acdX*
315 mutants the transcriptomes of these two mutants were compared to the wild-type
316 (**Supplemental Data 2, Supplemental Figure 4**). In the absence of olorofim 510 and 137
317 genes were respectively downregulated and upregulated in the Δ*devR* isolate while 212 were
318 downregulated and 194 upregulated upon olorofim exposure. In the absence of olorofim,
319 notable enriched functional categories included downregulation of genes involved in tyrosine
320 metabolism and an upregulation of genes involved in the biosynthesis of branched chain amino
321 acids and metabolism of arginine and proline, the latter of which was also seen under olorofim
322 exposure (**Figure 4a**). A detailed pathway analysis of genes involved in the conversion of
323 metabolites towards L-glutamate and through to orotate revealed that proline uptake and
324 degradation were upregulated in the *devR* null mutant (**Figure 4c**). Other pathways that
325 contribute to orotate precursors were also significantly upregulated, notably the nitrate
326 assimilation pathway (NAP [*crnA, niaD, niiA*]), and glutamate, glutamine and carbomyl-P
327 synthesis. Pathways that compete with orotidine biosynthesis for L-glutamate were not
328 differentially regulated in any of the assessed mutants (**Supplemental Figure 5).** Our
329 transcriptional data therefore suggests that nitrogen metabolism maybe altered in this strain in
330 ways that favor the generation of precursors for orotate biosynthesis and hence could explain
331 the reduced sensitivity of *devR* null mutant to olorofim.
332 The transcriptome of the olorofim hypersensitive Δ*acdX* mutant also revealed that proline and
333 arginine metabolism were upregulated compared to the wild-type however genes involved in
334 the NAP and glutamate, glutamine and carbomyl-P synthesis pathways were downregulated
335 suggesting that AcdX and DevR have directly opposing functions on these linked pathways
336 (**Figure 4d**) and providing further evidence to suggest that regulation of these pathways is
337 important for olorofim sensitivity.

338 Our transcriptomic data led us to assess the effect of pyrimidine pathway precursors on
339 olorofim susceptibility in the transcripton factor null mutants (**Supplemental Figure 6)**. Using
340 nitrate as the most abundant, but not sole nitrogen source increases susceptibility of *A.*
341 *fumigatus* MFIG001 to olorofim. Interestingly this increase in susceptibility is lost in the
342 Δ*devR*, perhaps as a consequence of the upregulation of the NAP in this mutant. In keeping
343 with this, the resistance phenoptype observed with the loss of AreA, a regulator that activates
344 the NAP, is lost. The hypersensitive phenotype in the *acdX* null mutant was exaggerated when
345 arginine and proline were used as sole nitrogen sources. These data, combined with results
346 from our transcriptomic analysis suggest that modification of environmental nitrogen sources
347 and or dysregulation of nitrogen metabolism is directly linked to changes in olorofim
348 sensitivity.

349 ***A clinical isolate with an hapE allele known to contribute to azole resistance does not affect***
350 ***olorofim sensitivity.***

351 HapB is a member of the heterotrimeric CBC complex along with HapE and HapC. We have
352 previously shown that this complex negatively regulates sterol biosynthesis and loss of any
353 member of this complex leads to azole resistance in *A. fumigatus* [22]. As the Δ*hapB* mutant
354 exhibited an olorofim resistance phenotype, we assessed the olorofim susceptibility for a
355 clinical isolate (V067-36) which has non-synonomous SNP in the *hapE* gene (resulting in a
356 P88L substitution) and which has been demonstrated to affect azole susceptibility. The MIC of
357 this isolate and an isogenic isolate with a wild-type *hapE* allele from the same patient were
358 identical for olorofim. To further confirm that the $hapE^{P88L}$ allele did not impact olorofim
359 susceptibility, we reconstructed this point mutation in the MFIG001 background. While a
360 Δ*hapB* mutant showed decreased susceptibility to both olorofim and itraconazole, the
361 MFIG001 $hapE^{P88L}$ strain only showed decreased susceptibility to itraconazole (**Figure 5**).

362 ***The action of the azoles and olorofim are antagonistic.***

363 As we have identified two genes whose loss of function can result in cross resistance, we
364 assessed if both drugs when used in combination would be synergistic against the respective
365 mutants. We first evaluated the potential synergism of both compounds against the isotype
366 control MFIG001. To our surprise given the distinct mechanisms of action of the orotomides
367 and the azoles, we observed a clear antagonism between itraconazole and olorofim. The
368 antagonism also persisted in the Δ*hapB,* the V067-36 isolate and the $hapE^{P88L}$ isolate (**Figure**
369 **5**). We evaluated our previously published RNA-seq data to assess if itraconazole increased
370 expression of genes involved in olorofim biosynthesis however contrary to our expectations,
371 many of the genes in the pyrimidine biosynthetic pathway were highly downregulated, even
372 when itraconazole was used at low levels **(Supplemental Data 1**).
373 We assessed if the antagonism persisted in multiple genetic backgrounds and to an alternative
374 azole (voriconazole). Consistent with our previous observations the wild-type isolate CEA10,
375 which is the parental strain from which MFIG001 derived, the ATCC46645 isolate and an azole
376 resistant isolate with the TR_{34} L98H allele isolated from a patient, all showed an antagonistic
377 relationship between olorofim and voriconazole (**Figure 6**). Interestingly our data suggests that
378 the antagonism is predominantly unidirectional, with the azoles inhibiting the action of
379 olorofim in both solid and liquid media for all strains.
380
381

382 **Discussion**

383 Olorofim is a novel antifungal, currently in phase 3 clinical trials. It has a broad spectrum of
384 activity against most moulds and acts by inhibiting the pyrimidine biosynthetic pathway
385 through disruption of DHODH activity [7]. Our preliminary analysis of the inhibitory effects
386 of olorofim revealed that the MIC and the IC50 were separated over a relatively large
387 concentration range (5-fold). This contrasts with what is seen with itraconazole and other
388 azoles where this concentration spread is typically 2-fold. The clinical implication of this
389 finding remains unclear, however it is likely that olorofim will support clearance of an infection
390 at doses well below the MIC. At these lower concentrations however, exposure to drug will be
391 imparting selective pressure and has the potential to induce the production of mutagenic
392 precursors that may drive the emergence of resistance as has been shown for several antibiotics
393 [39]. As with other anti-infectives that act by inhibiting a single biological target there is clear
394 potential for emergence of resistance. Understanding these mechanisms will provide a
395 framework for development of diagnostics to detect resistance rapidly in the clinic.

396 Our previous survey of azole sensitivity in the *A. fumigatus* COFUN transcription factor
397 knockout library [22] revealed 6 null mutants that had decreased sensitivity (ranging from 4 to
398 6-fold increase in MIC compared to the isogenic control) and 6 had increased sensitivity (4 to
399 8-fold decrease in MIC) to itraconazole. Here our screen revealed that only 1 mutant (Δ*acdX*)
400 showed increased sensitivity while 3 showed decreased sensitivity (Δ*hapB*, Δ*devR*, Δ*areA*) to
401 olorofim and the changes in sensitivity in these isolates were less extreme than seen for the
402 azoles. It is unsurprising, given the mechanism of action of olorofim, that the transcription
403 factors that we have identified in this screen either have well defined roles in regulating
404 nitrogen utilisation or have been linked to this function in our study.

405 What is remarkable however given the distinct mechanisms of actions of the two compound
406 classes, loss of function of either of AreA and HapB results in cross-class resistance to both

407 the azoles and orotomides. HapB is a member of the heterotrimeric CCAAT-binding complex
408 (CBC) and alongside HapC and HapE regulates the expression of over a third of the genome
409 [40] including several genes involved in ergosterol biosynthesis. The *hapB* null displayed the
410 highest levels of resistance to olorofim and was able to germinate at 0.12 mg/L, which is 8-
411 fold higher than the parental isolate but within the concentration range needed for clinical
412 utility. In *A. nidulans* AreA is a positive regulator of many genes that are required for utilisation
413 of nitrogen sources other than glutamate or ammonia [41] with loss of function resulting in an
414 inability to utilise amongst other nitrogen sources, nitrate, nitrite, uric acid and many amino
415 acids [42]. Reassuringly however, drug concentrations in animal models are tolerated well
416 above the increased MIC levels of the null mutants identified in this screen. Dosing 8 mg/kg at
417 8 hour intervals in mice results in peak serum levels of 2.5-3 mg/L [43]. Olorofim can be
418 tolerated at doses as high as 30 mg/kg intravenously, giving scope for higher drug levels *in*
419 *vivo* if required. In cynomolgus monkeys a single oral dose of olorofim resulted in peak levels
420 of 0.605-0.914 mg/L in serum for female and male animals, respectively [44].
421 Recently a clinical isolate, V067-36, has been described that harbours a mutant HapE allele
422 ($HapE^{P88L}$) which directly contributes to azole resistance [24]. Even though this mutation
423 appears to affect the way the CBC interacts with its gDNA target, independent of other co-
424 factors [40, 45, 46] our data shows that this allele does not affect susceptibility of *A. fumigatus*
425 to olorofim and is therefore less important at regulating a response to the orotomides. It is also
426 noteworthy that to date, no further documented cases of azole resistance have been linked to
427 CBC function and even though AreA is partially dispensable for virulence in *A. fumigatus* [41],
428 no cases of clinical resistance have been linked to AreA function. Therefore, although
429 concerning, the cross-resistance phenotypes we have observed may not have major clinical
430 significance. If olorofim is ultimately licenced for use, monitoring for co-resistance before
431 switching therapy would be a sensible precaution.

432 Our studies have shown there is a clear antagonism of the azoles and olorofim. Whilst
433 concerning the antagonism is only evident when relatively low levels of both drugs are used.
434 It is interesting to note that the TR_{34} L98H isolate used in this study has reduced susceptibility
435 to olorofim when compared to the CEA10 isolate and the antagonism drives the MIC above
436 0.5 mg/L. If these drugs are to be used in combination in a clinical setting, careful evaluation
437 of respective drug levels at the site of infection to ensure sufficient concentration of drug to
438 avoid antagonism would be sensible. The consequences of using azoles and olorofim in
439 combination for treatment of strains harbouring the TR_{34} L98H allele also needs further
440 evaluation.

441 In summary, we have explored the mechanism behind olorofim susceptibility through
442 a systematic analysis of the COFUN transcription factor null library. All the mutants we
443 identified that had altered sensitivity to olorofim have associated defects in nitrogen
444 metabolism and two of these mutants Δ*devR* and Δ*acdX* regulate genes involved in metabolic
445 pathways immediately upstream of the pyrimidine pathway potentially leading to a differential
446 flux of metabolites into this pathway. Although we have identified two transcription factors,
447 the CBC and AreA, that regulate cross resistance to both the azoles and olorofim we are
448 reassured that the only recognised incidence of clinical azole resistance linked to CBC function
449 (HapE P88L) does not lead to olorofim resistance.

450

451 **References**

452 1. Bongomin, F., et al., *Global and Multi-National Prevalence of Fungal Diseases-*
453 *Estimate Precision.* J Fungi (Basel), 2017. **3**(4).
454 2. Patterson, T.F., et al., *Practice Guidelines for the Diagnosis and Management of*
455 *Aspergillosis: 2016 Update by the Infectious Diseases Society of America.* Clin Infect
456 Dis, 2016. **63**(4): p. e1-e60.
457 3. Snelders, E., et al., *Possible environmental origin of resistance of Aspergillus fumigatus*
458 *to medical triazoles.* Appl Environ Microbiol, 2009. **75**(12): p. 4053-7.
459 4. van Rhijn, N. and M. Bromley, *The Consequences of Our Changing Environment on*
460 *Life Threatening and Debilitating Fungal Diseases in Humans.* Journal of Fungi, 2021.
461 **7**(5): p. 367.
462 5. Maertens, J.A., et al., *Isavuconazole versus voriconazole for primary treatment of*
463 *invasive mould disease caused by Aspergillus and other filamentous fungi (SECURE):*
464 *a phase 3, randomised-controlled, non-inferiority trial.* Lancet, 2016. **387**(10020): p.
465 760-9.
466 6. Rauseo, A.M., et al., *Hope on the Horizon: Novel Fungal Treatments in Development.*
467 Open Forum Infect Dis, 2020. **7**(2): p. ofaa016.
468 7. Oliver, J.D., et al., *F901318 represents a novel class of antifungal drug that inhibits*
469 *dihydroorotate dehydrogenase.* Proc Natl Acad Sci U S A, 2016. **113**(45): p. 12809-
470 12814.
471 8. Hope, W.W., et al., *Pharmacodynamics of the Orotomides against Aspergillus*
472 *fumigatus: New Opportunities for Treatment of Multidrug-Resistant Fungal Disease.*
473 mBio, 2017. **8**(4).
474 9. Boschi, D., et al., *Dihydroorotate dehydrogenase inhibitors in anti-infective drug*
475 *research.* Eur J Med Chem, 2019. **183**: p. 111681.

476 10. du Pre, S., et al., *The Dynamic Influence of Olorofim (F901318) on the Cell*
477 *Morphology and Organization of Living Cells of Aspergillus fumigatus.* J Fungi
478 (Basel), 2020. **6**(2).
479 11. du Pre, S., et al., *Effect of the Novel Antifungal Drug F901318 (Olorofim) on Growth*
480 *and Viability of Aspergillus fumigatus.* Antimicrob Agents Chemother, 2018. **62**(8).
481 12. Biswas, C., et al., *In vitro activity of the novel antifungal compound F901318 against*
482 *Australian Scedosporium and Lomentospora fungi.* Med Mycol, 2018. **56**(8): p. 1050-
483 1054.
484 13. Kirchhoff, L., et al., *Antibiofilm activity of antifungal drugs, including the novel drug*
485 *olorofim, against Lomentospora prolificans.* J Antimicrob Chemother, 2020.
486 14. Lim, W., et al., *Madurella mycetomatis, the main causative agent of eumycetoma, is*
487 *highly susceptible to olorofim.* J Antimicrob Chemother, 2020. **75**(4): p. 936-941.
488 15. Seyedmousavi, S., et al., *Efficacy of Olorofim (F901318) against Aspergillus*
489 *fumigatus, A. nidulans, and A. tanneri in Murine Models of Profound Neutropenia and*
490 *Chronic Granulomatous Disease.* Antimicrob Agents Chemother, 2019. **63**(6).
491 16. Wiederhold, N.P., D. Law, and M. Birch, *Dihydroorotate dehydrogenase inhibitor*
492 *F901318 has potent in vitro activity against Scedosporium species and Lomentospora*
493 *prolificans.* J Antimicrob Chemother, 2017. **72**(7): p. 1977-1980.
494 17. Wiederhold, N.P., et al., *The Orotomide Olorofim Is Efficacious in an Experimental*
495 *Model of Central Nervous System Coccidioidomycosis.* Antimicrob Agents Chemother,
496 2018. **62**(9).
497 18. Lackner, M., et al., *Dihydroorotate dehydrogenase inhibitor olorofim exhibits*
498 *promising activity against all clinically relevant species within Aspergillus section*
499 *Terrei.* J Antimicrob Chemother, 2018. **73**(11): p. 3068-3073.

500 19. Buil, J.B., et al., *In vitro activity of the novel antifungal compound F901318 against*
501 *difficult-to-treat Aspergillus isolates.* J Antimicrob Chemother, 2017. **72**(9): p. 2548-
502 2552.
503 20. Rivero-Menendez, O., M. Cuenca-Estrella, and A. Alastruey-Izquierdo, *In vitro activity*
504 *of olorofim (F901318) against clinical isolates of cryptic species of Aspergillus by*
505 *EUCAST and CLSI methodologies.* J Antimicrob Chemother, 2019. **74**(6): p. 1586-
506 1590.
507 21. Jorgensen, K.M., et al., *EUCAST Determination of Olorofim (F901318) Susceptibility*
508 *of Mold Species, Method Validation, and MICs.* Antimicrob Agents Chemother, 2018.
509 **62**(8).
510 22. Furukawa, T., et al., *The negative cofactor 2 complex is a key regulator of drug*
511 *resistance in Aspergillus fumigatus.* Nat Commun, 2020. **11**(1): p. 427.
512 23. Bertuzzi, M., et al., *On the lineage of Aspergillus fumigatus isolates in common*
513 *laboratory use.* Med Mycol, 2020.
514 24. Camps, S.M., et al., *Discovery of a HapE mutation that causes azole resistance in*
515 *Aspergillus fumigatus through whole genome sequencing and sexual crossing.* PLoS
516 One, 2012. **7**(11): p. e50034.
517 25. van Rhijn, N., et al., *Development of a marker-free mutagenesis system using CRISPR-*
518 *Cas9 in the pathogenic mould Aspergillus fumigatus.* Fungal Genetics and Biology,
519 2020. **145**: p. 103479.
520 26. Rodriguez-Tudela, J.L., et al., *Epidemiological cutoffs and cross-resistance to azole*
521 *drugs in Aspergillus fumigatus.* Antimicrob Agents Chemother, 2008. **52**(7): p. 2468-
522 72.
523 27. Berman, J. and D.J. Krysan, *Drug resistance and tolerance in fungi.* Nat Rev Microbiol,
524 2020. **18**(6): p. 319-331.

525 28. Barratt, R.W., G.B. Johnson, and W.N. Ogata, *Wild-type and mutant stocks of*
526 *Aspergillus nidulans.* Genetics, 1965. **52**(1): p. 233-46.
527 29. Bolger, A.M., M. Lohse, and B. Usadel, *Trimmomatic: a flexible trimmer for Illumina*
528 *sequence data.* Bioinformatics, 2014. **30**(15): p. 2114-20.
529 30. Howe, K.L., et al., *Ensembl Genomes 2020-enabling non-vertebrate genomic research.*
530 Nucleic Acids Res, 2020. **48**(D1): p. D689-D695.
531 31. Love, M.I., W. Huber, and S. Anders, *Moderated estimation of fold change and*
532 *dispersion for RNA-seq data with DESeq2.* Genome Biol, 2014. **15**(12): p. 550.
533 32. Priebe, S., et al., *FungiFun2: a comprehensive online resource for systematic analysis*
534 *of gene lists from fungal species.* Bioinformatics, 2015. **31**(3): p. 445-6.
535 33. Odds, F.C., *Synergy, antagonism, and what the chequerboard puts between them.*
536 Journal of Antimicrobial Chemotherapy, 2003. **52**(1): p. 1-1.
537 34. Soothill, J.S., R. Ward, and A.J. Girling, *The IC50: an exactly defined measure of*
538 *antibiotic sensitivity.* J Antimicrob Chemother, 1992. **29**(2): p. 137-9.
539 35. Amaar, Y.G. and M.M. Moore, *Mapping of the nitrate-assimilation gene cluster (crnA-*
540 *niiA-niaD) and characterization of the nitrite reductase gene (niiA) in the opportunistic*
541 *fungal pathogen Aspergillus fumigatus.* Curr Genet, 1998. **33**(3): p. 206-15.
542 36. Hortschansky, P., et al., *Deciphering the combinatorial DNA-binding code of the*
543 *CCAAT-binding complex and the iron-regulatory basic region leucine zipper (bZIP)*
544 *transcription factor HapX.* J Biol Chem, 2015. **290**(10): p. 6058-70.
545 37. Sermwittayawong, D. and S. Tan, *SAGA binds TBP via its Spt8 subunit in competition*
546 *with DNA: implications for TBP recruitment.* EMBO J, 2006. **25**(16): p. 3791-800.
547 38. Georgakopoulos, P., R.A. Lockington, and J.M. Kelly, *SAGA complex components and*
548 *acetate repression in Aspergillus nidulans.* G3 (Bethesda), 2012. **2**(11): p. 1357-67.

549 39. Kohanski, M.A., M.A. DePristo, and J.J. Collins, *Sublethal antibiotic treatment leads*
550 *to multidrug resistance via radical-induced mutagenesis.* Mol Cell, 2010. **37**(3): p. 311-
551 20.
552 40. Gsaller, F., et al., *Sterol Biosynthesis and Azole Tolerance Is Governed by the Opposing*
553 *Actions of SrbA and the CCAAT Binding Complex.* PLoS Pathog, 2016. **12**(7): p.
554 e1005775.
555 41. Hensel, M., et al., *The role of the Aspergillus fumigatus areA gene in invasive*
556 *pulmonary aspergillosis.* Mol Gen Genet, 1998. **258**(5): p. 553-7.
557 42. Arst, H.N. and D.J. Cove, *Nitrogen metabolite repression in Aspergillus nidulans.*
558 Molecular and General Genetics MGG, 1973. **126**(2): p. 111-141.
559 43. Hope, W.W., et al., *Pharmacodynamics of the orotomides against Aspergillus*
560 *fumigatus: new opportunities for treatment of multidrug-resistant fungal disease.*
561 MBio, 2017. **8**(4).
562 44. Law, D., et al. *Pharmacokinetics of the Novel Antifungal Agent F901318 in Mice, Rats*
563 *and Cynomolgus monkey*. in *Fifty-fifth Interscience Conference on Antimicrobial*
564 *Agents and Chemotherapy. San Diego, California*. 2015.
565 45. Furukawa, T., et al., *The fungal CCAAT-binding complex and HapX display highly*
566 *variable but evolutionary conserved synergetic promoter-specific DNA recognition.*
567 Nucleic acids research, 2020. **48**(7): p. 3567-3590.
568 46. Hortschansky, P., et al., *The CCAAT-binding complex (CBC) in Aspergillus species.*
569 Biochim Biophys Acta, 2017. **1860**(5): p. 560-570.

570

571 **Figure 1: The response of *A. fumigatus* to olorofim.** (a) MIC of *A. fumigatus* MFIG001 to
572 olorofim as measured by OD_{600} by EUCAST methodology. (b) Addition of 10mM uracil and
573 10mM uridine reverses the action of olorofim to *A. fumigatus* MFIG001 (n=3). (c) Volcano
574 plot of RNA-seq of *A. fumigatus* A1160p+ exposed to olorofim. 185 genes (blue dots) and 41
575 genes (red dots) were considered downregulated and upregulated, respectively (>2-fold
576 differentially regulated, $p<0.05$). (d) KEGG pathways that are enriched within differentially
577 regulated genes, blue categories are associated with downregulated genes, red with upregulated
578 genes. (e) Interactions of proteins involved in response to olorofim as determined by
579 StringsDB. Proteins derived from upregulated transcripts are in red, downregulated in blue.
580 **Figure 2: Olorofim susceptibility screening of the COFUN transcription factor knockout**
581 **library.** (a) Relative fitness of each individual strain was assessed by normalising to fitness in
582 non-drug condition (n=3). TF null mutants that are of particular interest are highlighted. (b-e)
583 MIC to olorofim of the TF null mutants, (b) for Δ*acdX*, (c) for Δ*hapB*, (d) for Δ*devR*, (e) for
584 Δ*areA*, as determined by OD_{600} (n=3). Statistical difference was assessed by Two-way
585 ANOVA with Sidaks multiple comparison test (* $p<0.05$, ** $p<0.01$, *** $p<0.001$, ***
586 $p<0.001$).
587 **Figure 3: Phenotypic evaluation of TF null mutants.** (a) 500 spores of TF null mutants and
588 MFIG001+ were spotted on Aspergillus Complete Medium and Aspergillus Minimal Medium
589 and incubated for 48 hours at 37º Celsius. (b-c) Radial growth of TF null mutants and A1160p+
590 on ACM (b) and AMM (c), after 72 hours at 37º Celsius (n=3) (d) TF null mutants spotted on
591 AMM supplemented with 50 mM ammonium tartrate, 10 mM sodium nitrate, 10 mM L-
592 glutamine, 10 mM urea or 10 mM L-proline (n=3) Statistical difference was assessed by two-
593 way ANOVA with Dunn's correction (p-values < 0.05 are shown).
594 **Figure 4: RNA-seq analysis of Δ*devR* and Δ*acdX* exposed to olorofim.** (a) KEGG pathways
595 enriched for down- (blue) or upregulated (red) genes in RPMI-1640 or upon olorofim exposure

596 for Δ*devR* compared to *A. fumigatus* A1160p+. (b) KEGG pathways enriched for down- (blue)
597 or upregulated (red) genes in RPMI-1640 or upon olorofim exposure for Δ*acdX* compared to
598 *A. fumigatus* A1160p+. (c) Detailed analysis of genes involved in pathways upstream of and
599 including the pyrimidine pathway. The target of olorofim, DHODH, is highlighted. Blue is
600 more than 1-fold downregulated, yellow more than 1-fold upregulated; red is more than 5-fold
601 upregulated. The right of each box is associated with Δ*acdX*, left with Δ*devR*. (d) Heatmap of
602 genes involved in the pyrimidine pathway and component upstream of this pathway.

603 **Figure 5: Checkerboard assays for CBC complex associated strains.** Checkerboard assays
604 were performed (n=3) by using a double dilution series of itraconazole (16-0.06 mg/L) along
605 the X-axis and olorofim (0.5-0.003 mg/L) along the Y-axis. The Δ*hapB* and hapE^{P88L} isolates
606 are in the MFIG001 background, the V067-36 isolate is a clinical isolate containing the P88L
607 point mutation within HapE. The FICI is shown in the right top corner of each individual plot
608 to show the antagonistic effect. Values greater than 4 indicate antagonism.

609 **Figure 6: The antagonistic effect between voriconazole and olorofim.** (a) Checkerboard
610 assays were performed (n=2) by using a double dilution series of voriconazole (16-0.06 mg/L)
611 along the X-axis and olorofim (0.500-0.007 mg/L) along the Y-axis. Two wild-type isolates
612 (CEA10 and ATCC46645) were assessed and an azole resistant TR_{34} L98H isolate. The FICI
613 is shown in the right top corner of each individual plot to show the antagonistic effect. (b)
614 Representative images of disk assays of the CEA10, ATCC46645 and TR_{34} L98H isolates to
615 voriconazole and olorofim. A clear disruption of the olorofim halo can be observed proximal
616 to the voriconazole halo.

617 **Supplemental Figure 1: Microscopical evaluation of *A. fumigatus* MFIG001 and**
618 **transcription factor null mutants upon olorofim exposure.** Representative images were
619 taken from the MIC 96-well plates by stereomicroscope. Maximum concentration at which
620 growth is observed is highlighted in black for each strain.

621 **Supplemental Figure 2: Determination of IC50 for itraconazole**. MIC to olorofim in RPMI-
622 1640 was determined according to EUCAST methodology for *A. fumigatus* MFIG001. OD600
623 was measured after 48 hours to determine growth quantitatively.
624 **Supplemental Figure 3: Images of nitrogen spot tests of TF null mutants.** Growth of TF
625 null mutants and wild-type was assessed on AMM supplemented with 50 mM ammonium
626 tartrate, 10 mM sodium nitrate, 10 mM L-glutamine, 10 mM urea or 10 mM L-proline (n=3).
627 Images were taken after 72 hours at 37 Celsius.
628 **Supplemental Figure 4: Volcano plots of Δ*acdX* and Δ*devR* RNA-seq data.** Volcano plots
629 showing $\log_2$(Fold-Change) compared to A1160p+ on the X-axis and $-\log_{10}$(False Discovery
630 Rate) from DESeq2 on the Y-axis. Genes considered differentially regulated are coloured in
631 red, and number of genes differentially regulated are noted in each respective corner of volcano
632 plots.
633 **Supplemental Figure 5: Pathways utilising L-glutamate.** Additional pathways utilising L-
634 glutamate. Genes involved in these reactions are shown, none of these were differentially
635 regulated in Δ*acdX* or Δ*devR*.
636 **Supplemental Figure 6: Olorofim MICs in supplemental RPMI-1640**. MICs according to
637 EUCAST methodology in RPMI-1640 supplemented with 20 mM arginine, 10 mM nitrate, 20
638 mM proline or 50 mM glutamine. Addition of nitrate changed Olorofim susceptibility by 2-
639 fold for all strains except Δ*devR*.
640 **Supplemental Table 1**: **Oligos and crRNA used in this study.**
641

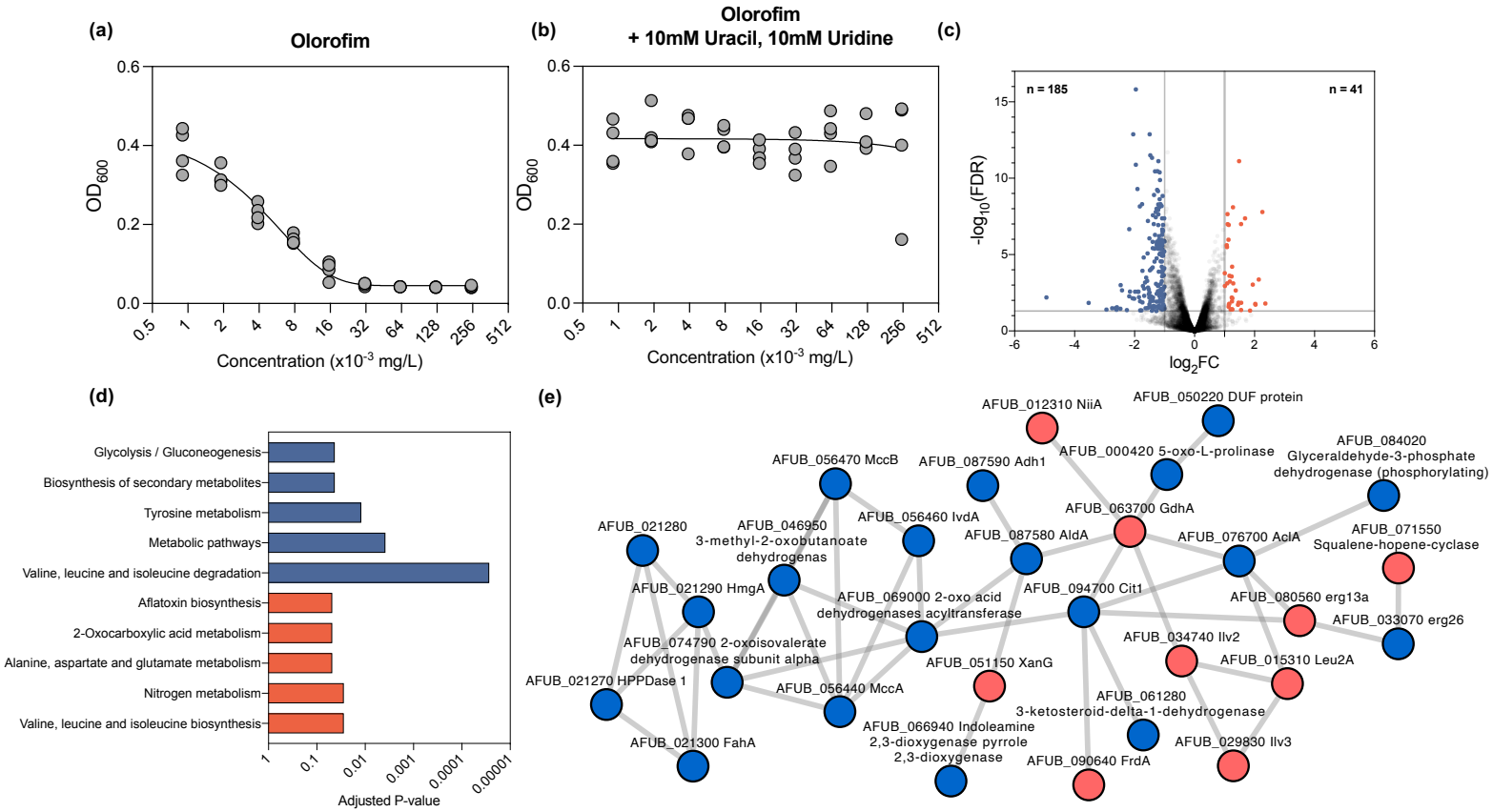
(a)
Olorofim
OD600
Concentration (x10-3 mg/L)
(b)
Olorofim
+ 10mM Uracil, 10mM Uridine
OD600
Concentration (x10-3 mg/L)
(c)
n = 185
n = 41
-log10(FDR)
log2FC
(d)
Glycolysis / Gluconeogenesis
Biosynthesis of secondary metabolites
Tyrosine metabolism
Metabolic pathways
Valine, leucine and isoleucine degradation
Aflatoxin biosynthesis
2-Oxocarboxylic acid metabolism
Alanine, aspartate and glutamate metabolism
Nitrogen metabolism
Valine, leucine and isoleucine biosynthesis
Adjusted P-value
(e)
AFUB_012310 NiiA
AFUB_050220 DUF protein
AFUB_000420 5-oxo-L-prolinase
AFUB_084020 Glyceraldehyde-3-phosphate dehydrogenase (phosphorylating)
AFUB_056470 MccB
AFUB_087590 Adh1
AFUB_063700 GdhA
AFUB_056460 IvdA
AFUB_021280
AFUB_046950 3-methyl-2-oxobutanoate dehydrogenas
AFUB_087580 AldA
AFUB_076700 AclA
AFUB_071550 Squalene-hopene-cyclase
AFUB_021290 HmgA
AFUB_069000 2-oxo acid dehydrogenases acyltransferase
AFUB_094700 Cit1
AFUB_080560 erg13a
AFUB_033070 erg26
AFUB_074790 2-oxoisovalerate dehydrogenase subunit alpha
AFUB_034740 Ilv2
AFUB_051150 XanG
AFUB_015310 Leu2A
AFUB_021270 HPPDase 1
AFUB_056440 MccA
AFUB_061280 3-ketosteroid-delta-1-dehydrogenase
AFUB_066940 Indoleamine 2,3-dioxygenase pyrrole 2,3-dioxygenase
AFUB_021300 FahA
AFUB_029830 Ilv3
AFUB_090640 FrdA

643

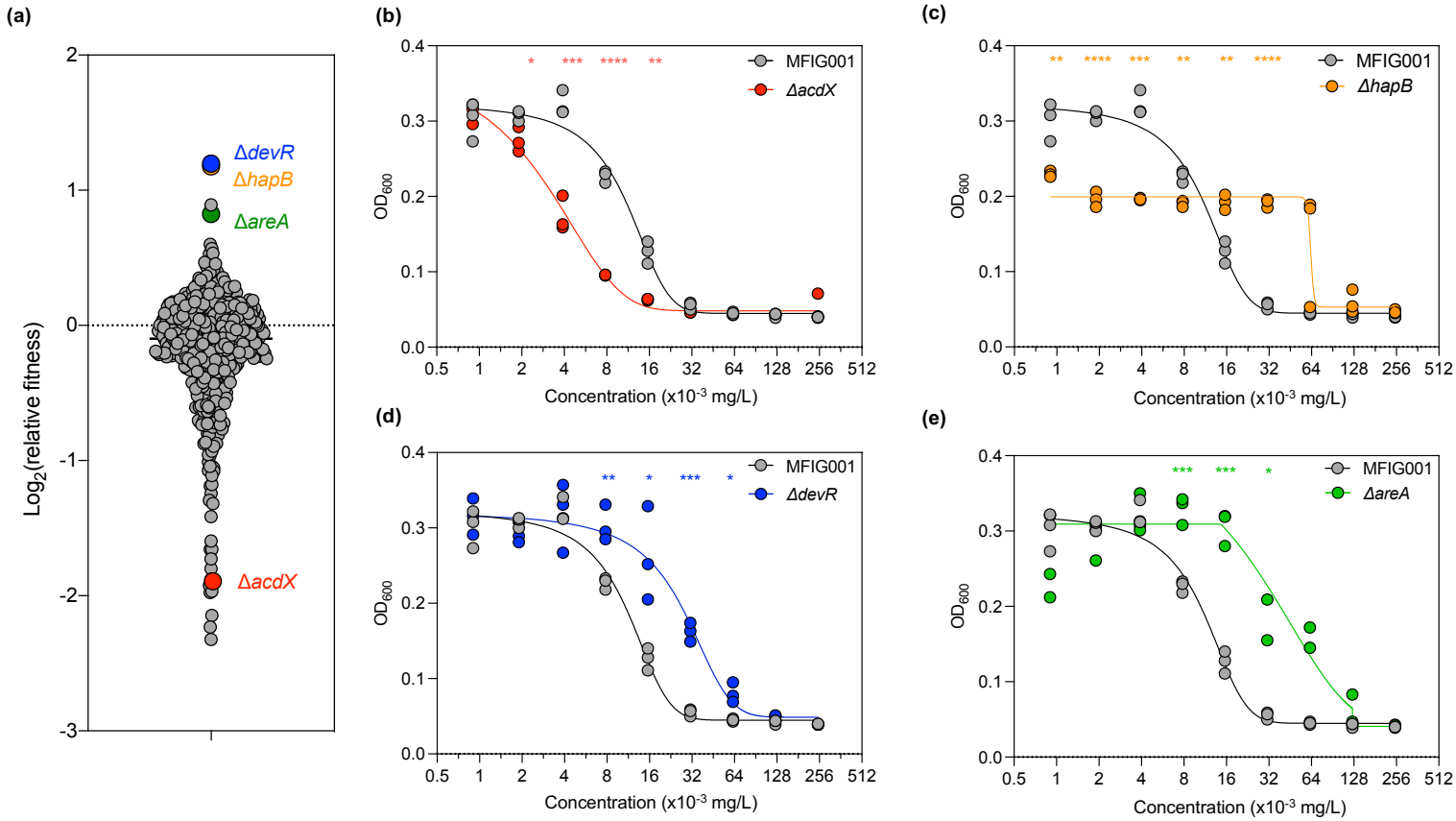
(a)
ΔdevR
ΔhapB
ΔareA
ΔacdX
Log2(relative fitness)
(b)
MFIG001
ΔacdX
OD600
Concentration (x10-3 mg/L)
(c)
MFIG001
ΔhapB
(d)
MFIG001
ΔdevR
(e)
MFIG001
ΔareA

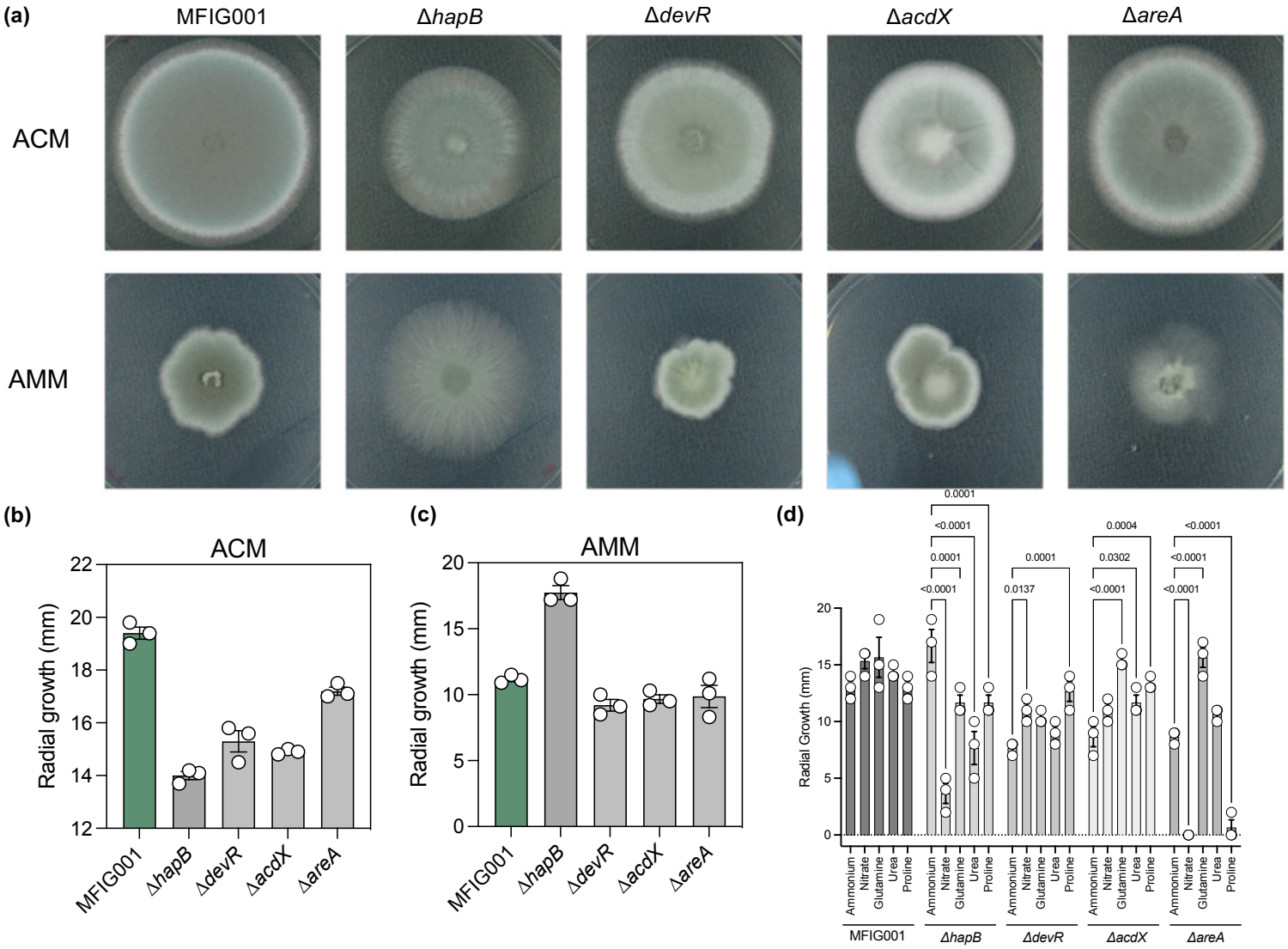
(a)
MFIG001
ΔhapB
ΔdevR
ΔacdX
ΔareA
ACM
AMM
(b)
ACM
Radial growth (mm)
22
20
18
16
14
12
MFIG001
ΔhapB
ΔdevR
ΔacdX
ΔareA
(c)
AMM
Radial growth (mm)
20
15
10
5
0
MFIG001
ΔhapB
ΔdevR
ΔacdX
ΔareA
(d)
Radial Growth (mm)
20
15
10
5
0
0.0001
<0.0001
0.0001
<0.0001
0.0001
0.0137
0.0004
0.0302
<0.0001
<0.0001
<0.0001
<0.0001
Ammonium
Nitrate
Glutamine
Urea
Proline
MFIG001
ΔhapB
ΔdevR
ΔacdX
ΔareA

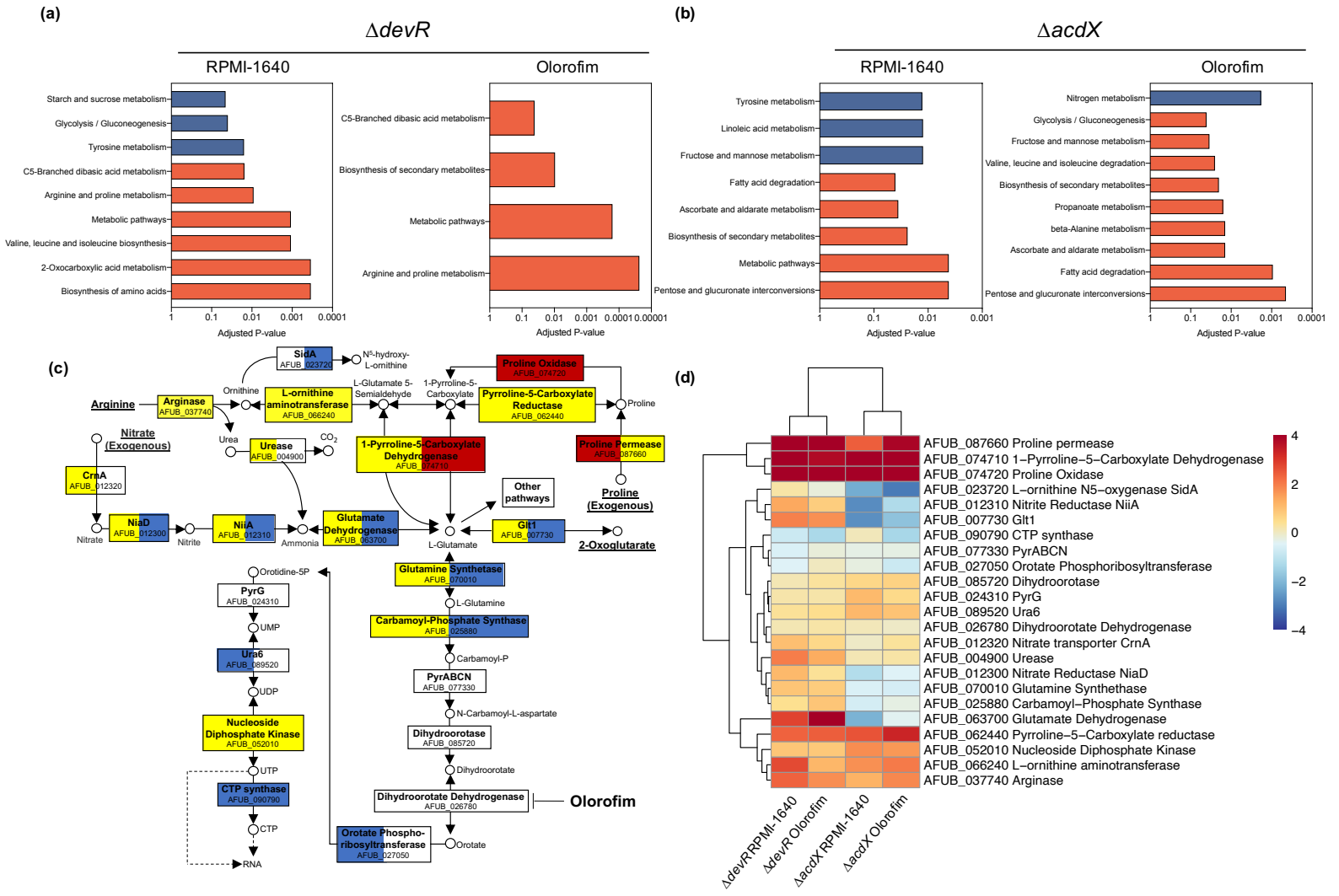
(a)
ΔdevR
RPMI-1640
Olorofim
Starch and sucrose metabolism
Glycolysis / Gluconeogenesis
Tyrosine metabolism
C5-Branched dibasic acid metabolism
Arginine and proline metabolism
Metabolic pathways
Valine, leucine and isoleucine biosynthesis
2-Oxocarboxylic acid metabolism
Biosynthesis of amino acids
C5-Branched dibasic acid metabolism
Biosynthesis of secondary metabolites
Metabolic pathways
Arginine and proline metabolism
Adjusted P-value
(b)
ΔacdX
RPMI-1640
Olorofim
Tyrosine metabolism
Linoleic acid metabolism
Fructose and mannose metabolism
Fatty acid degradation
Ascorbate and aldarate metabolism
Biosynthesis of secondary metabolites
Metabolic pathways
Pentose and glucuronate interconversions
Nitrogen metabolism
Glycolysis / Gluconeogenesis
Fructose and mannose metabolism
Valine, leucine and isoleucine degradation
Biosynthesis of secondary metabolites
Propanoate metabolism
beta-Alanine metabolism
Ascorbate and aldarate metabolism
Fatty acid degradation
Pentose and glucuronate interconversions
Adjusted P-value
(c)
Arginine
Arginase AFUB_037740
Ornithine
SidA AFUB_023720
N5-hydroxy-L-ornithine
L-ornithine aminotransferase AFUB_066240
L-Glutamate 5-Semialdehyde
1-Pyrroline-5-Carboxylate
Proline Oxidase AFUB_074720
Pyrroline-5-Carboxylate Reductase AFUB_062440
Proline
Nitrate (Exogenous)
Urea
Urease AFUB_004900
CO2
1-Pyrroline-5-Carboxylate Dehydrogenase AFUB_074710
Proline Permease AFUB_087660
Proline (Exogenous)
CrnA AFUB_012320
Other pathways
Nitrate
NiaD AFUB_012300
Nitrite
NiiA AFUB_012310
Ammonia
Glutamate Dehydrogenase AFUB_063700
L-Glutamate
Glt1 AFUB_007730
2-Oxoglutarate
Orotidine-5P
PyrG AFUB_024310
UMP
Ura6 AFUB_089520
UDP
Nucleoside Diphosphate Kinase AFUB_052010
UTP
CTP synthase AFUB_090790
CTP
RNA
Glutamine Synthetase AFUB_070010
L-Glutamine
Carbamoyl-Phosphate Synthase AFUB_025880
Carbamoyl-P
PyrABCN AFUB_077330
N-Carbamoyl-L-aspartate
Dihydroorotase AFUB_085720
Dihydroorotate
Dihydroorotate Dehydrogenase AFUB_026780
Olorofim
Orotate Phospho-ribosyltransferase AFUB_027050
Orotate
(d)
AFUB_087660 Proline permease
AFUB_074710 1−Pyrroline−5−Carboxylate Dehydrogenase
AFUB_074720 Proline Oxidase
AFUB_023720 L−ornithine N5−oxygenase SidA
AFUB_012310 Nitrite Reductase NiiA
AFUB_007730 Glt1
AFUB_090790 CTP synthase
AFUB_077330 PyrABCN
AFUB_027050 Orotate Phosphoribosyltransferase
AFUB_085720 Dihydroorotase
AFUB_024310 PyrG
AFUB_089520 Ura6
AFUB_026780 Dihydroorotate Dehydrogenase
AFUB_012320 Nitrate transporter CrnA
AFUB_004900 Urease
AFUB_012300 Nitrate Reductase NiaD
AFUB_070010 Glutamine Synthethase
AFUB_025880 Carbamoyl−Phosphate Synthase
AFUB_063700 Glutamate Dehydrogenase
AFUB_062440 Pyrroline−5−Carboxylate reductase
AFUB_052010 Nucleoside Diphosphate Kinase
AFUB_066240 L−ornithine aminotransferase
AFUB_037740 Arginase
ΔdevR RPMI-1640
ΔdevR Olorofim
ΔacdX RPMI-1640
ΔacdX Olorofim

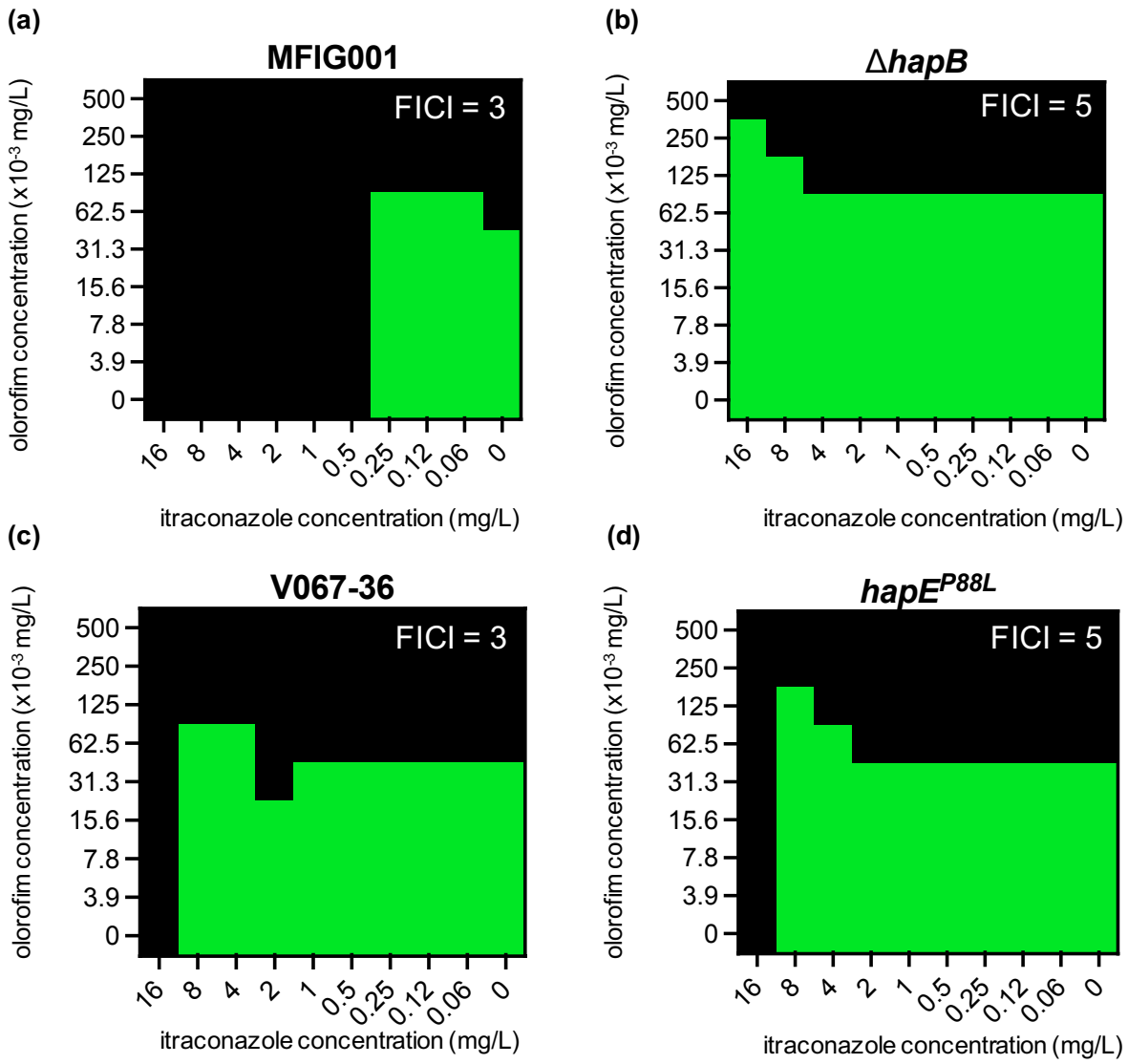
(a)
MFIG001
FICI = 3
olorofim concentration (x10-3 mg/L)
500
250
125
62.5
31.3
15.6
7.8
3.9
0
16 8 4 2 1 0.5 0.25 0.12 0.06 0
itraconazole concentration (mg/L)
(b)
ΔhapB
FICI = 5
olorofim concentration (x10-3 mg/L)
500
250
125
62.5
31.3
15.6
7.8
3.9
0
16 8 4 2 1 0.5 0.25 0.12 0.06 0
itraconazole concentration (mg/L)
(c)
V067-36
FICI = 3
olorofim concentration (x10-3 mg/L)
500
250
125
62.5
31.3
15.6
7.8
3.9
0
16 8 4 2 1 0.5 0.25 0.12 0.06 0
itraconazole concentration (mg/L)
(d)
hapEP88L
FICI = 5
olorofim concentration (x10-3 mg/L)
500
250
125
62.5
31.3
15.6
7.8
3.9
0
16 8 4 2 1 0.5 0.25 0.12 0.06 0
itraconazole concentration (mg/L)

646

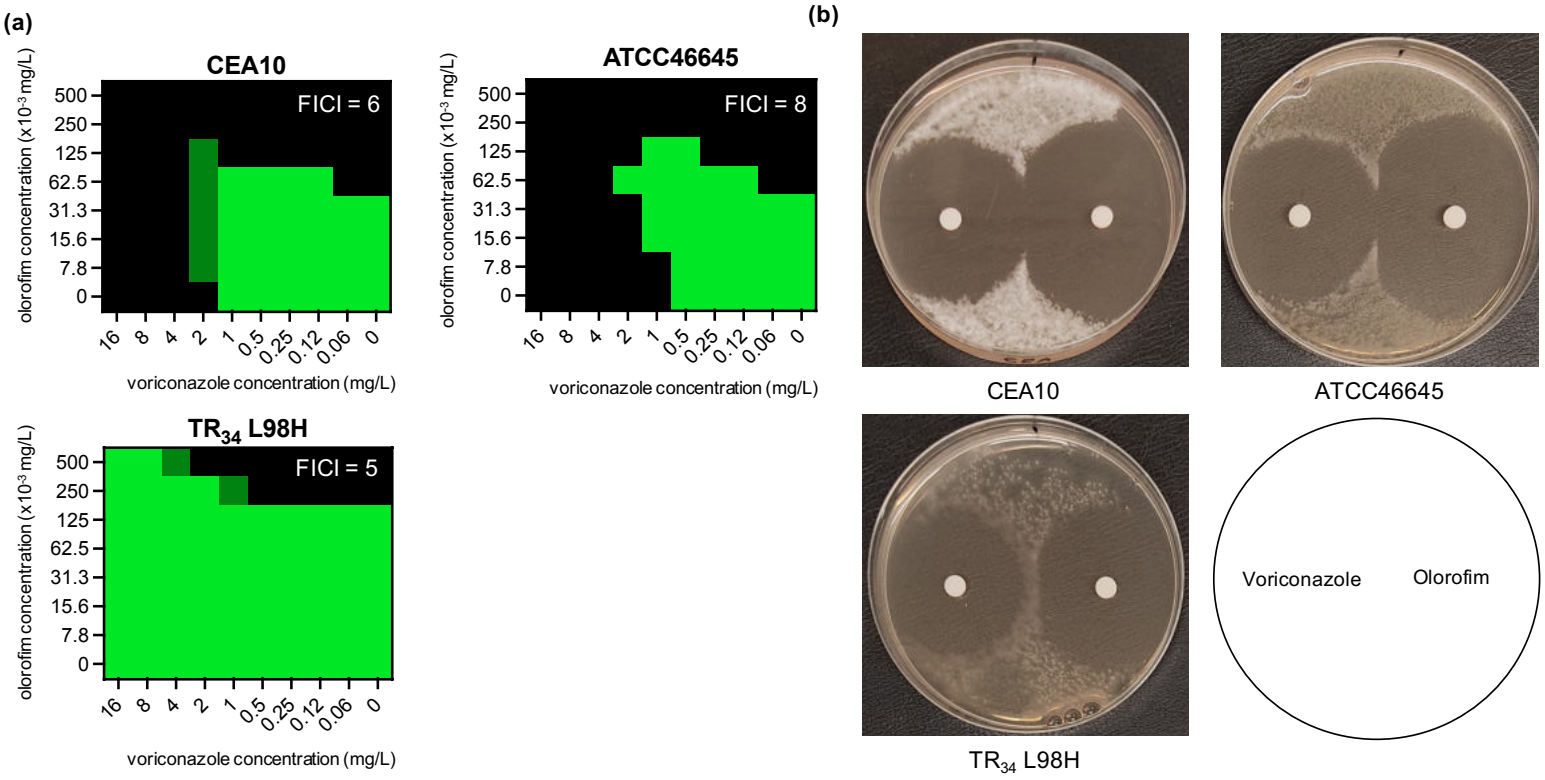
(a)
CEA10
FICI = 6
ATCC46645
FICI = 8
TR34 L98H
FICI = 5
olorofim concentration (x10-3 mg/L)
500
250
125
62.5
31.3
15.6
7.8
0
16 8 4 2 1 0.5 0.25 0.12 0.06 0
voriconazole concentration (mg/L)
(b)
CEA10
ATCC46645
TR34 L98H
Voriconazole
Olorofim

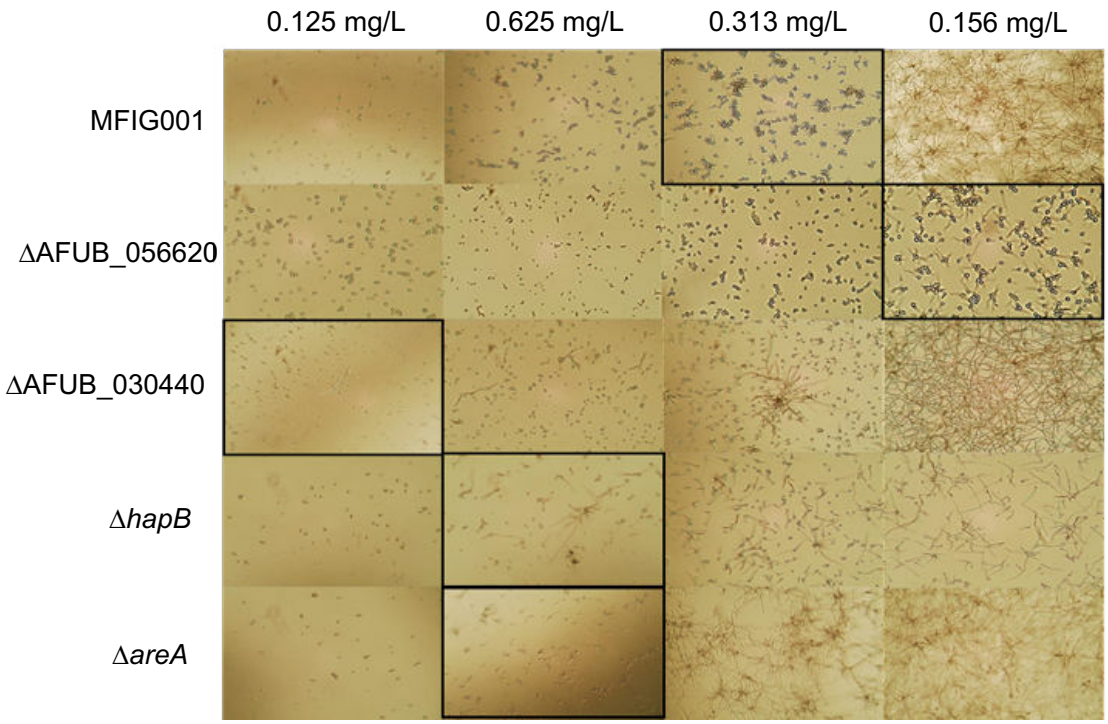
0.125 mg/L
0.625 mg/L
0.313 mg/L
0.156 mg/L
MFIG001
ΔAFUB_056620
ΔAFUB_030440
Δ*hapB*
Δ*areA*

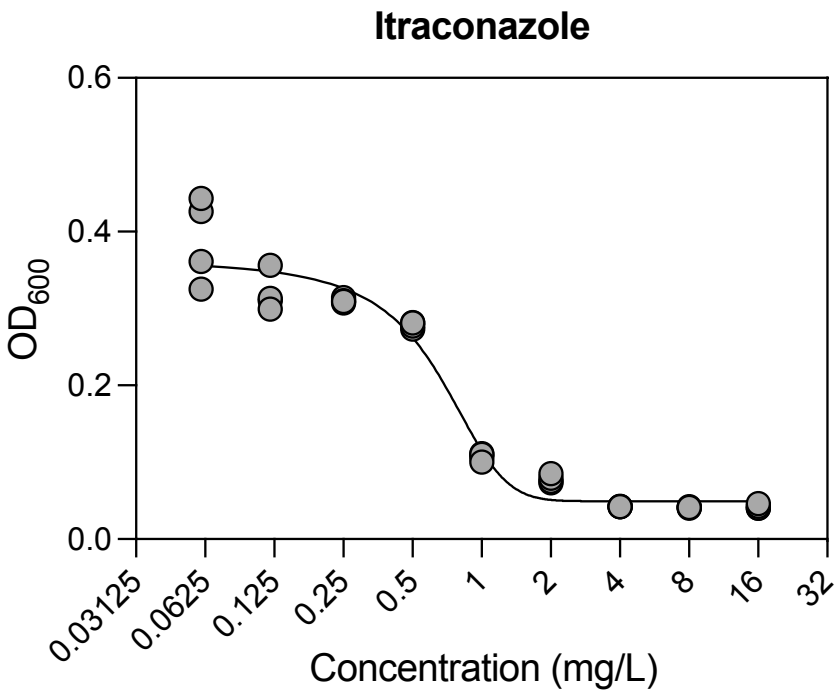
Itraconazole
0.6
0.4
0.2
0.0
OD600
0.03125
0.0625
0.125
0.25
0.5
1
2
4
8
16
32
Concentration (mg/L)

649

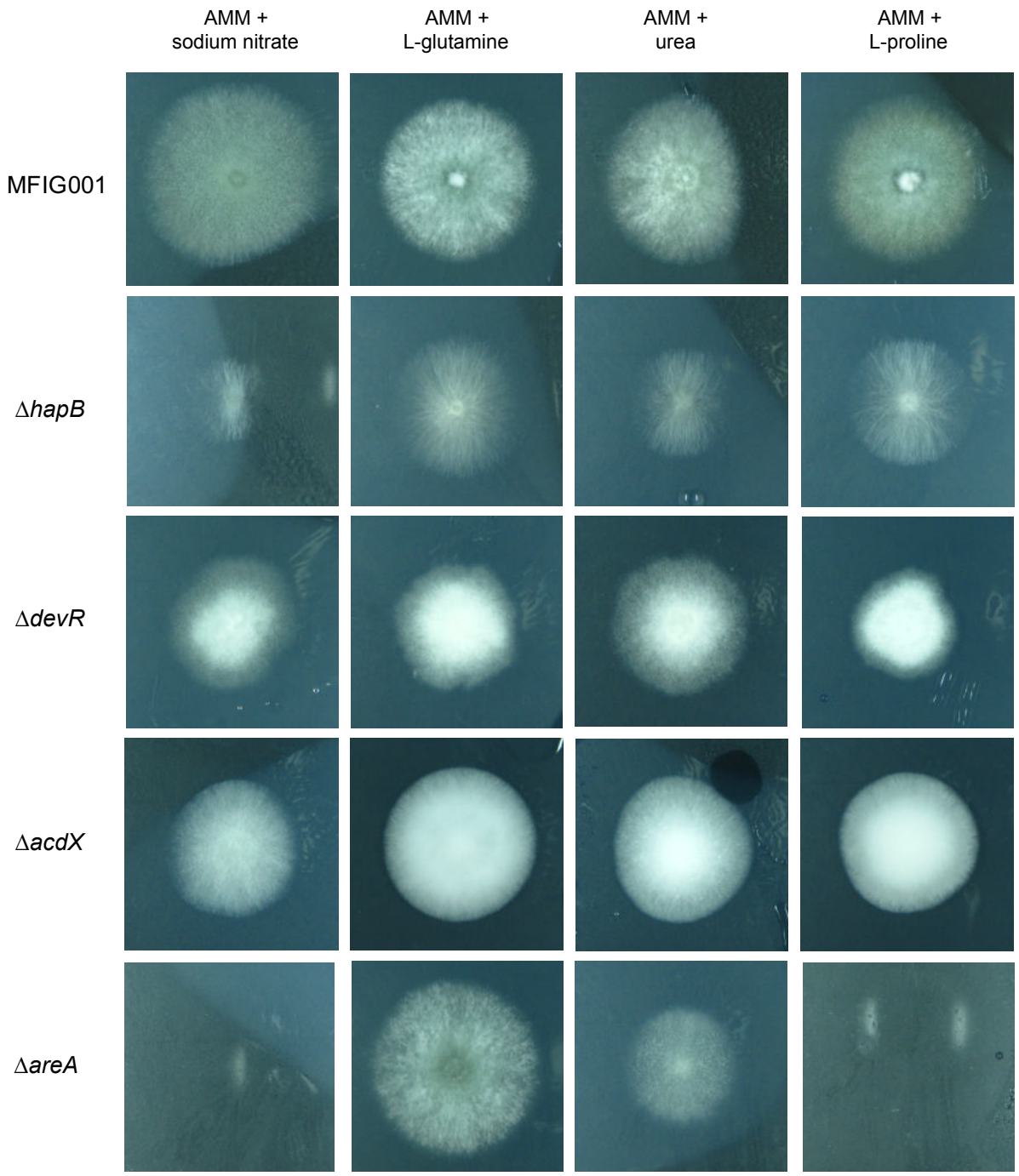
AMM +
sodium nitrate
AMM +
L-glutamine
AMM +
urea
AMM +
L-proline
MFIG001
Δ*hapB*
Δ*devR*
Δ*acdX*
Δ*areA*

650

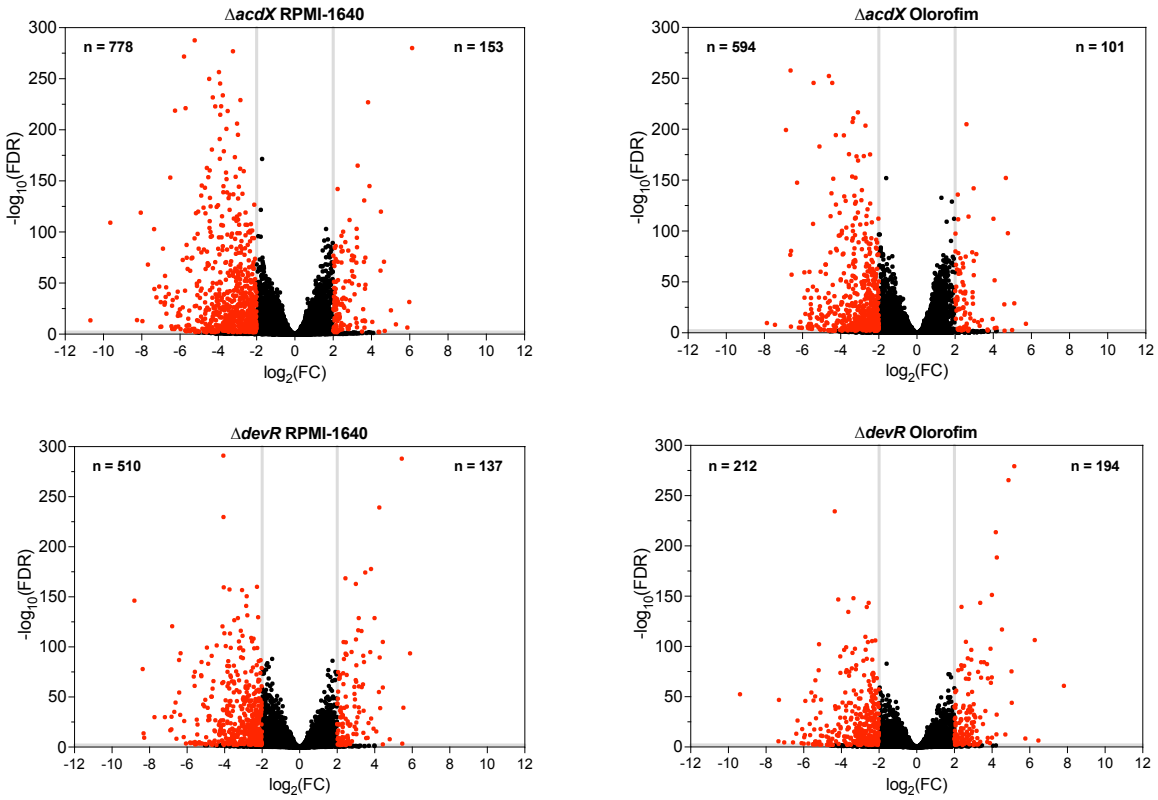
ΔacdX RPMI-1640
n = 778
n = 153
ΔacdX Olorofim
n = 594
n = 101
ΔdevR RPMI-1640
n = 510
n = 137
ΔdevR Olorofim
n = 212
n = 194
-log10(FDR)
log2(FC)

651

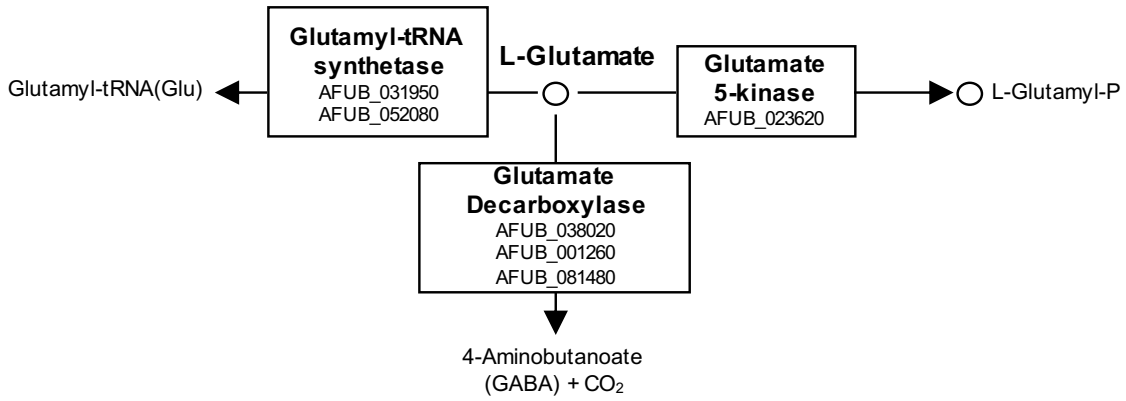
Glutamyl-tRNA synthetase
AFUB_031950
AFUB_052080
L-Glutamate
Glutamate 5-kinase
AFUB_023620
Glutamyl-tRNA(Glu)
L-Glutamyl-P
Glutamate Decarboxylase
AFUB_038020
AFUB_001260
AFUB_081480
4-Aminobutanoate
(GABA) + CO2

652

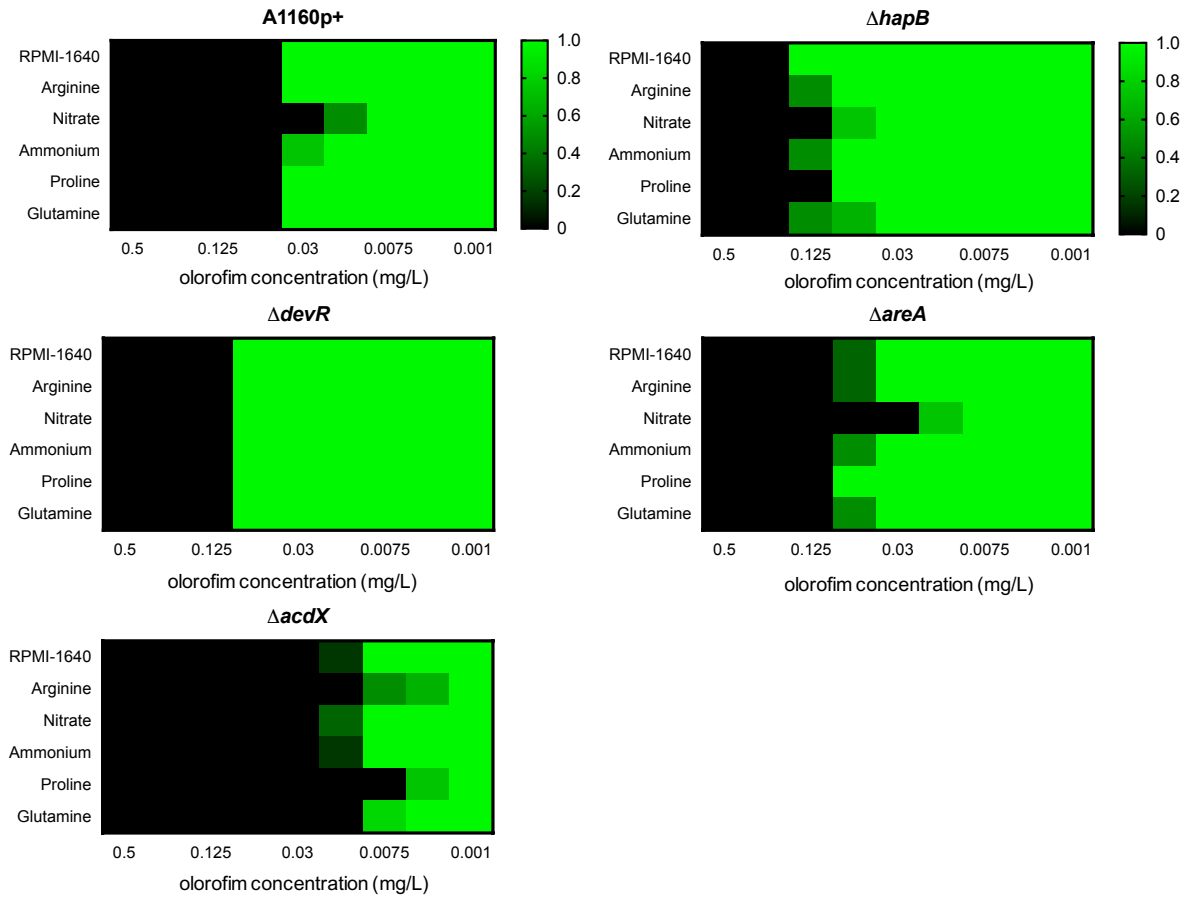
A1160p+
RPMI-1640
Arginine
Nitrate
Ammonium
Proline
Glutamine
0.5
0.125
0.03
0.0075
0.001
olorofim concentration (mg/L)
1.0
0.8
0.6
0.4
0.2
0
Δhapb
Δdevr
Δareas
Δacdx

653

654

Oligo name	Oligo sequence (5 to 3')
hapE_gene_Fw	AGCTCTATCCAGCTGAAGTG
hapE_gene_Rv	AGATTTCTCTCGCTGACTGA
hapE_Fw	TCAAGGGCTACAAGGCACAG
hapE_Rv	AGATATCGCAGCCTTTCGCA
hapE_Seq	CCGCGACATACTAACGACCT
hapE_392_revcom	ATAGGTCGTTAGTATGTCGC

655